Appl. Phys. B 87, 151–156 (2007)
DOI: 10.1007/s00340-006-2536-z

Applied Physics B
Lasers and Optics

H.L. XU[1,✉]
G. MÉJEAN[1]
W. LIU[1]
Y. KAMALI[1]
J.-F. DAIGLE[1]
A. AZARM[1]
P.T. SIMARD[1]
P. MATHIEU[2]
G. ROY[2]
J.-R. SIMARD[2]
S.L. CHIN[1]

Remote detection of similar biological materials using femtosecond filament-induced breakdown spectroscopy

[1] Centre d'Optique, Photonique et Laser (COPL) et Département de Physique, de Génie Physique et d'Optique, Université Laval, Québec, QC, G1K 7P4, Canada
[2] Optronic Surveillance, Defense Research and Development Canada-Valcartier, 2459 Pie-XI Blvd North, Québec, QC, G3J 1X5, Canada

Received: 2 October 2006
Published online: 16 December 2006 •

ABSTRACT We demonstrated the feasibility of remote detection and differentiation of some very similar agricultural-activity related bioaerosols, namely barley, corn, and wheat grain dusts, through nonlinear fluorescence of fragments induced by the high-intensity inside filaments of femtosecond laser pulses in air. The signals were detected in Lidar configuration with targets located at 4.7 m away from the detection system. All the species showed identical spectra, namely those from molecular C_2 and CN bands, as well as atomic Si, C, Mg, Al, Na, Ca, Mn, Fe, Sr and K lines. These identical spectral bands and lines reveal similar chemical compositions; however, the relative intensities of the spectra are different showing different element abundances from these three bio-targets. The intensity ratios of different elemental lines were used to distinguish these three samples. Good reproducibility was obtained. We expect that this technique could be used at long distance and thus played as a sensor of similar biological hazards for public and defense security.

PACS 42.68.Wt; 95.75.Fg

1 Introduction

Laser-induced breakdown spectroscopy (LIBS), which is based on the emission spectroscopy of materials ablated into a small plasma by a tightly focused laser beam, is a powerful tool for on-line, real-time material elemental analysis [1–3]. The spectral lines of the emission spectrum provide information on the chemical composition of the sample, and the line intensities can reveal the relative abundances of the elements in the sample. LIBS has found applications in areas such as analytical chemistry, industrial process on-line control, environmental monitoring, and cultural heritage imaging and diagnostics [4–6].

In recent years, LIBS using femtosecond pulses (Femto-LIBS) has attracted much attention [7–9]. The plasma induced by a femtosecond pulse has very different properties than those generated by a longer pulse. In the long (nanosecond) laser pulse regime, the plasma is generated by multiphoton ionization (MPI) and/or tunnel ionization (TI) [10] followed by inversed Bremsstrahlung and avalanche (collisions) ionization. The plasma plume ejected from the surface is further heated by the long laser pulse, resulting in a hot plasma. This total ionization gives rise to atomic lines superimposed on a plasma continuum. However, in the case of a femtosecond laser pulse, the interaction is only limited to the surface involving MPI and/or TI and some collisional ionization. Because of the very short interaction time, the laser pulse is already gone before the plasma plume is ejected from the surface. Thus, the plasma temperature is low. As a result, in comparison with nanosecond LIBS (ns-LIBS), femto-LIBS has a low-intensity continuum in the emission spectra [11]. In addition, the high focused intensity in the interaction region because of the short pulse duration leads to a lower breakdown threshold energy in femto-LIBS; this in turn leads to more precise ablation and minimal invasive detection. For remote elemental analysis, femto-LIBS has an additional advantage in delivering high laser intensities over long distances to induce a plasma breakdown on the sample by utilizing the filamentation phenomenon induced by nonlinear propagation of femtosecond laser pulses in air [12]. According to the slice-by-slice self-focusing scenario described in the moving focus model [13], filamentation occurs because of the dynamical balance between the self-focusing induced by the optical Kerr effect and the defocusing effect of self-generated weak plasma at self-focus. After the laser pulse has gone, the series of self-foci will leave behind a plasma channel, popularly called filament. During the filamentation process, the equilibrium between the self-focusing and plasma defocusing will give rise to a limited laser peak intensity as well as a limited filament diameter. This characteristic of femtosecond laser pulse propagation is known as intensity clamping (about 5×10^{13} W/cm^2 in air) (see e.g., [13] and references therein). So far, the filamentation at a distance as far as a few kilometers in the atmosphere has been observed [14].

The purpose of this work is mainly to remotely probe and distinguish biological samples in a laboratory environment using femtosecond filament-induced breakdown spectroscopy (FIBS) [15]. Previously, there are only few investigations described in the literature dedicated to the analysis of biological samples using FIBS [16]. However, the detection and identification of biological agents has recently become quite urgent because of biological threats to public and de-

✉ Fax: +1-418-656-2623, E-mail: huailiang.xu.1@ulaval.ca

fense security and epidemic spreads in the world [17–19]. In the present paper, using FIBS, we demonstrate laboratory scale 'remote' detection and differentiation between three examples of agricultural activities related bioaerosols whose FIBS characteristics are very similar, namely, barley, corn, and wheat grain dusts. The signals were detected in the backward direction. Molecular C_2 and CN bands, as well as atomic Si, C, Mg, Al, Na, Ca, Mn, Fe, Sr and K lines were recorded. These spectral bands and lines reveal almost identical chemical composition, but different element abundances from these three bio-targets. A kinetic analysis of the CN and C_2 bands reveal that the product of CN comes either from native CN dissociated directly from the samples and/or from the interaction between the laser-induced plasma and the ambient air; while the C_2 fluorescence results directly from native C_2 dissociated from the samples. The intensity ratios of different elemental lines were used to distinguish these three samples. The results allow us to propose that the FIBS technique could be used to remotely distinguish very similar biological materials.

2 Experimental setup

The experimental setup of the FIBS system is schematically illustrated in Fig. 1. A Ti:sapphire femtosecond laser system was used in the present experiment to ablate the materials. Pulses, emitted from a Ti:sapphire oscillator (Spectra Physics Tsunami) with 30-fs duration, were positively chirped to about 200 ps in a stretcher and amplified in a regenerative amplifier (Spectra Physics Spitfire). A 10-Hz pulse train extracted from the 1-kHz output of the regenerative amplifier was further amplified in a two-pass Ti:sapphire amplifier. A portable compressor was used to shorten the pulse duration, measured with a single shot autocorrelator (SSA Positive Light), to about 45 fs. The energy of the pulse was controlled by a half wave plate and a polarizer located before the amplifier that could be varied from 0.5 to 12 mJ. The compressed pulse spectrum is centered at 800 nm with a 23 nm bandwidth (FWHM) and the laser beam had a radius of $a \approx 2.7$ mm ($1/e$ level of intensity). As shown in Fig. 1, two dielectric mirrors (M1: diameter $d = 25.4$ mm and M2: $d = 76.2$ mm) with high reflectivity at around 800 nm were used to reflect the beam. The laser pulses were focused in air using a fused-silica lens (L1: $f = 1$ m, 2 or 5 m, thickness = 6.3 mm). The barley, corn, and wheat grain dust samples (Greer Laboratories) were compressed to form tablets using a mechanical compressor. The tablets were fixed on a rotating stage in order to prevent any destruction and aging of sample structures because of the sensitivity of the biological material to thermal shock induced by laser irradiation; this would also allow noninvasive measurements. The sample under study was placed 4 m away from M2 and perpendicular to the laser beam. The focal lens (L1) was placed in order to that the filament start between 0.2 and 0.5 m before the sample.

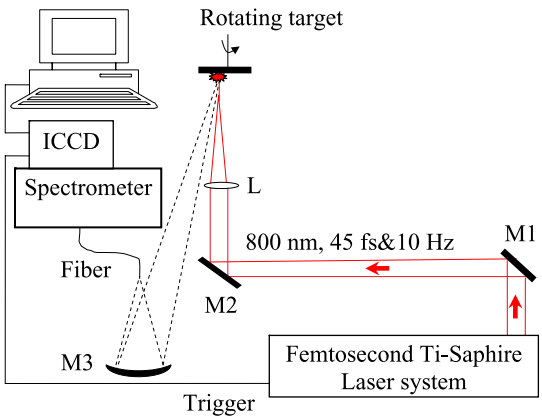

FIGURE 1 Experimental setup used for remote FIBS measurements

The fluorescence signal was observed in the backward direction; it was collected and focused, using a concave aluminum mirror (M3: $f = 1.5$ m, diameter 30 cm), onto a fiber bundle, which was coupled to a 0.5-m spectrometer (Acton Research Corp., SpectraPro-500i). The spectral resolution of the spectrometer was about 0.4 nm using a grating of 1200 grooves/mm (blazed wavelength at 500 nm) with 100 μm entrance slit width. The distance between the collection mirror M3 and the sample was about 4.7 m, which is limited by the size and other constraints of our laboratory. The dispersed fluorescence was detected by a gated intensified charge coupled device (ICCD, Princeton instruments Pi-Max 512), which can permit time-resolved spectral measurement with nanosecond precision. For fluorescence decay measurements, a Hamamatsu photomultiplier tube (PMT) with a rise time of 2 ns was connected to the spectrometer. A Tektronix digital phosphor oscilloscope (TDS 7254) with a bandwidth of 2.5 GHz was used to record and average the signals from the PMT.

3 Results and discussions

Figure 2 shows femtosecond filament-induced time-integrated breakdown spectra of barley (middle), corn (top) and wheat (bottom) grain dusts collected from the backward direction in the spectral range of 200–700 nm. The

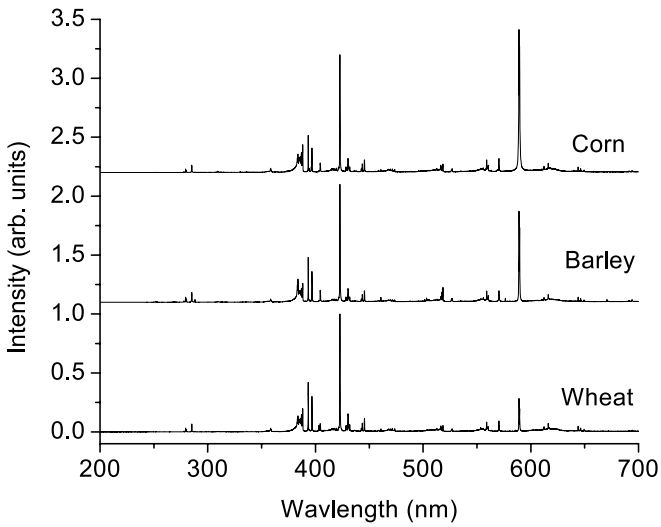

FIGURE 2 FIBS spectra obtained for the barley, corn, and wheat grain dusts with the delay of $t = 60$ ns with respect to the laser pulse on the target ($t = 0$). Laser pulse energy is 7 mJ and the ICCD gate width is 2 μs. The spectra are normalized to Ca I line at 422.67 nm and shifted in order to facilitate the observation

energy of a single pulse is 7 mJ. The ICCD gate width (detection window) was set to $\Delta t = 2\,\mu$s and the delay time was set to $t = 60$ ns after each laser pulse on the target ($t = 0$) so as to avoid the direct detection of the back scattered white light laser pulse associated to self-phase modulation and self-steepening of femtosecond laser pulse propagating in air [13, 20, 21]. The signal data were averaged over 200 laser shots. Here one can see that the femtosecond filament-induced UV-visible fluorescence spectra of these three bio-samples are very clean; that is, no continuum emissions are observed with a time delay of 60 ns. This hints a low temperature in the femtosecond laser-induced plasma. Without using such a delayed detection, the white light in the filament would be scattered back to the detection system, leading to a strong continuum band in the fluorescence spectra, as shown in Fig. 3. This spectrum was recorded for the barley grain dust sample with a time delay of $t = -3$ ns (minus means before the arrival of the laser pulse). The inset of Fig. 3 shows part of the spectrum of Fig. 3, but in a different scale. It can be seen from the inset of Fig. 3 that the white light (the band around 534 nm results from the grating's second-order diffraction of the third harmonic of the pump laser at 267 nm [22]) has masked the fluorescence signals emitted from the sample, although several spectral lines emitted from the samples can still be observed [23, 24]. It should be pointed out that the white light background cannot be eliminated by subtracting, like in the gas experiment [25], the background spectrum. This is because the white light background is not reproducible by introducing another target even if this target is nonfluorescing since the scattering characteristics of the two targets are different. Since the continuum emission in filament-induced spectra is dominantly due to the white light laser in air, the white-light contribution to the spectra due to filamentation can be easily damped out because of the short pulse duration of the white light laser (Fig. 2). These properties of FIBS are very favorable for detecting biological agents in practical applications because the detection window can be opened much earlier than in the scheme of classical ns-LIBS, thus the trace mineral elements and organic molecular bands can be detected in a higher contrast.

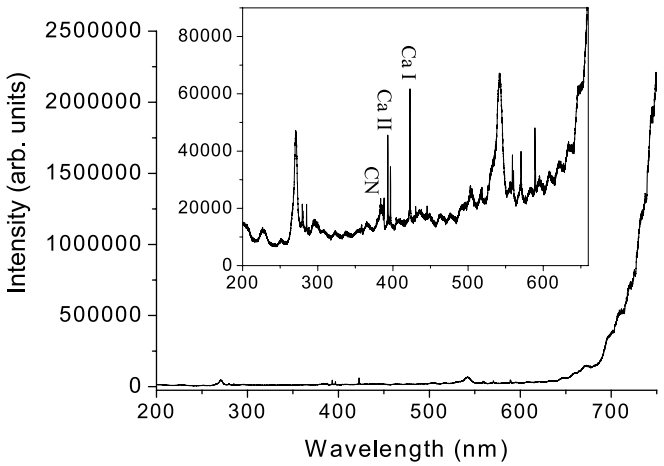

FIGURE 3 FIBS spectrum obtained for the barley grain dusts with the delay of $t = -3$ ns. The *inset* shows part of spectrum of Fig. 3 in a different scale

Figure 4 demonstrates the femtosecond filament-induced breakdown spectra of barley (red), corn (black) and wheat (blue) grain dusts in a higher-resolution scale. These spectra are normalized to the strongest Ca I line at 422.67 nm ($4s4p\,^1P_1{}^0 - 4s^2\,^1S_0$). Analysis of the plasma spectra shows that the emission comes from small molecular fragments (cyano radical: CN and dicarbon molecule: C_2), organic element (carbon: C I), as well as some mineral elements, including atomic and ionic magnesium (Mg I, Mg II) and calcium (Ca I, Ca II), atomic iron (Fe I), potassium (K I), sodium (Na I), silicon (Si I), strontium (Sr I), manganese (Mn I) and aluminum (Al I) [23, 24]. It should be pointed out that since the spectrometer resolution is limited, several spectral lines recorded in Fig. 4 are the ones including several atomic overlapping lines. For example, the line at 285.2 nm is related to four overlapping transitions of atomic Mg I at 285.1652, 285.1654, 285.166 and 285.213 nm, and the line 445.6 nm is formed by three overlapping transitions of atomic Ca I at 445.478, 445.589 and 445.662 nm. We also note that the molecular bands observed in the spectra, i.e., the CN ($B\,^2\Sigma^+ - X^2\Sigma^+$) violet system and the C_2 ($d^3\prod_g - a^3\prod_u$) Swan band system can be observed in all cases of barley, corn, and wheat dusts. The occurrence of C_2 might be directly derived from the connection of carboxyl group –COOH to carbon atom in amino acids (one of the basic components of a living cell) or from the C_2H_x fragments in aromatic ring, which are present in the samples, and might also come from carbon–carbon recombination in the plasma. As for the CN, it might possibly originate from the decomposition products present in the target compounds, such as the connection of amino group NH_2 or NH to carbon atoms in amino acids. However, it could also have come from the interaction of C_2 contained in the plume with N_2 from ambient air by the reaction $C_2 + N_2 \leftrightarrow 2CN$ [17]. In order to determine whether the CN and C_2 emissions originate from native CN and C_2 in the samples or not, we measured the decay profiles of CN and C_2 fluorescence by monitoring the luminescence at 388.25 and 469.73 nm, respectively. As an example, Fig. 5 shows the CN and C_2 fluorescence decays in a semi-logarithmic representation for the barley dust sample. In the two decays, the backgrounds have been subtracted, which were obtained by slightly tuning the detection wavelengths to off-resonant positions, i.e., 391 and 478 nm, respectively. It can be seen from Fig. 5 that the emission of CN molecular band exhibits a clear rise time of 20 ns after an initial sharp rise limited by the detector system (~ 2 ns), whereas that of C_2 molecular band has only a sharp rising profile. It should be pointed out that the CN and C_2 temporal profiles obtained in the corn and wheat samples show similar behaviors as in Fig. 5 (not shown). The sharp rise can be interpreted as being the 'immediate' fluorescence resulting from the direct interaction of the femtosecond laser pulse with the target. The rise time of this 'immediate' fluorescence is limited by the detector system's rise time. As suggested by Baudelet et al. [11, 19], the molecular emissions due to the interaction of the plasma and the ambient air can proceed later after the laser excitation. This would result in a slower rise of the fluorescence spectrum. Therefore, in the present experiments, it can be seen from Fig. 5 that the C_2 is due to the direct ablation of native C_2 from the samples, whereas CN originates from both the interaction of C_2 contained in the plume with N_2 from

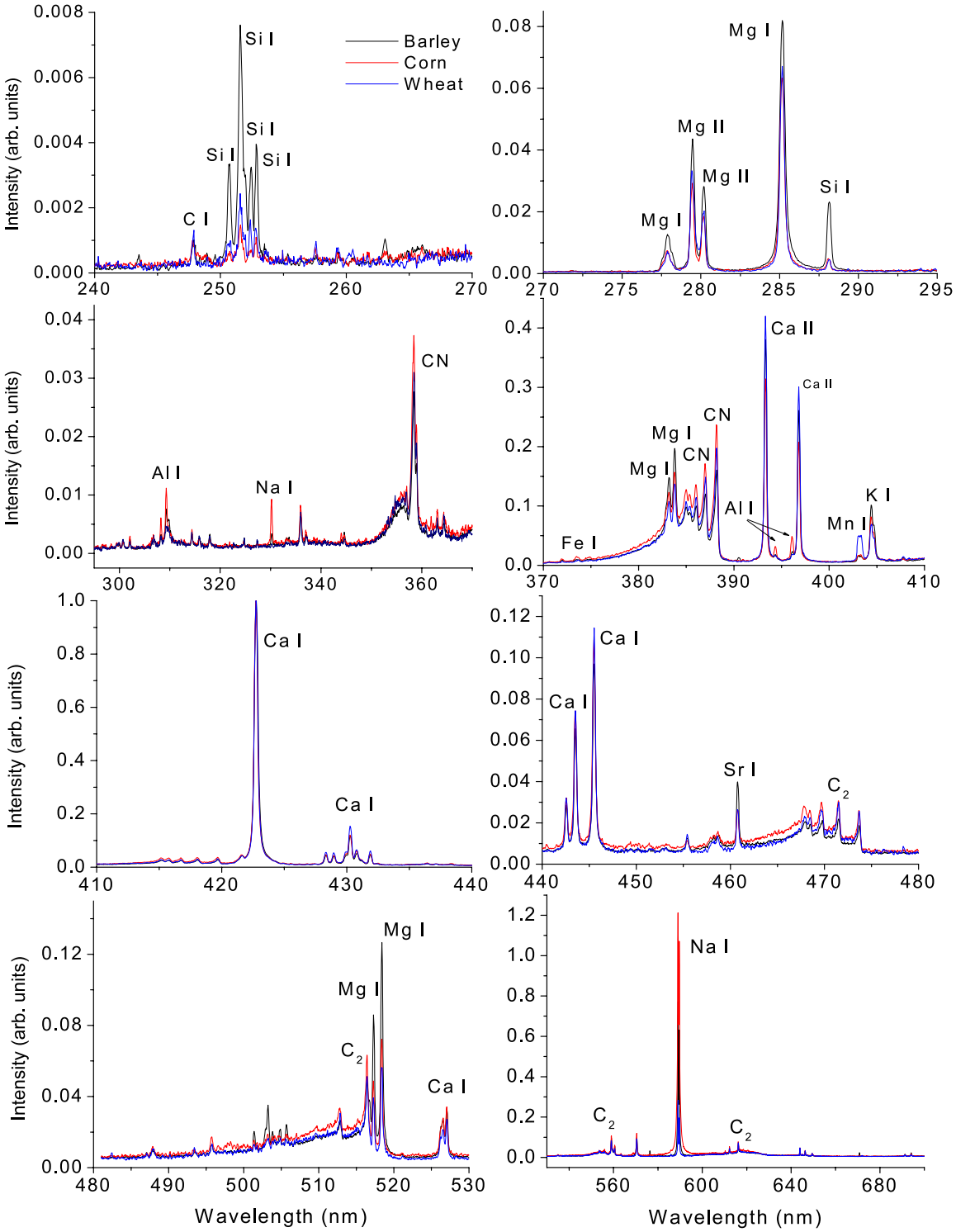

FIGURE 4 Time-resolved FIBS spectra in higher-resolution scales

ambient air by the reaction $C_2 + N_2 \leftrightarrow 2CN$ and the direct ablation of native CN from the samples.

According to the assignments of spectral lines and bands, we found that all of the elemental species observed in Fig. 4 are present in the barley, corn, and wheat grain dusts, indicating that they have similar chemical compositions. However, we can clearly see in Fig. 4 that the signal intensities of some spectral lines and bands are quite different. For example, the emissions from Mg I, II at 285.213 nm ($3s3p\,^1P_1{}^0 - 3s^2\,^1S_0$) and 279.553 nm ($3p\,^2P_{3/2}{}^0 - 3s\,^2S_{2/1}$) and from Si I at 288.158 nm ($3s^23p4s\,^1P_1{}^0 - 3s^23p^2\,^1D_2$) are significantly larger in the barley grain dust than in the corn and wheat grain dusts; Al I at 396.152 nm ($3s^2(^1S)4s\,^2S_{1/2} - 3s^2(^1S)3p\,^2P_{3/2}{}^0$) is much larger in the corn grain dust than in barley and wheat grain dusts; while Mn I at 403.076 nm ($3d^5(^6S)4s4p(^3P^0)z\,^6P_{7/2}{}^0 - 3d^54s^2a\,^6S_{5/2}$) is much smaller

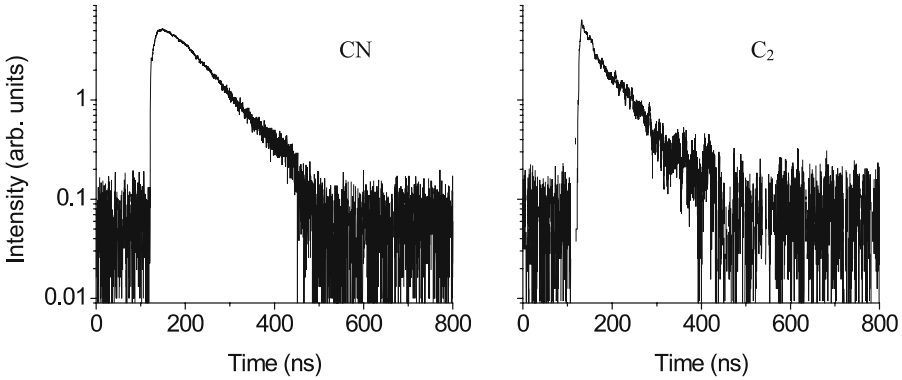

FIGURE 5 Decay profiles of the CN and C_2 molecular bands at 388.25 and 469.73 nm in a semilogarithmic representation for the barley sample

in the barley and corn grain dusts than in wheat grain dust. This suggests that these elemental abundances in these three bio-samples are quite different, which can be used to identify which biological sample is under investigation. However, as previously proposed [26], the sample identification with line intensity ratios is expected to be much better than with single line intensity because of better statistics.

The lines chosen to calculate line intensity ratios are those strongest transitions of elements in the spectra, including the atomic lines at 285.17 nm (Mg I), 288.16 nm (Si I), 396.15 nm (Al I), 403.31 nm (Mn I), 422.67 nm (Ca I), 588.99 nm (Na I), and the molecular bands at 388.25 nm (CN) and 516.41 (C2). An important aspect of remote sensing of pollutants is reproducibility. To determine the reproducibility of this method, we studied the line intensity ratios of the spectra under different experimental conditions, i.e., the focal lens ($f = 1$ m, 2 m and 5 m), as well as different measurement time (different days). In addition, in order to avoid the contamination produced by the manipulation of the sample, for each material, two samples were prepared independently for the measurements. Several line intensity ratios of these three samples obtained from the lines and bands of interest were summarized in Table 1. The line intensities were obtained by averaging the signals over 200 laser shots in order to decrease the shot-to-shot variations. The values obtained are the averaged ones with about six experimental measurements. The errors in Table 1 denote statistical uncertainties in the measurements. As can be seen from Table 1, these three bioaerosols can be easily distinguished. For instance, according to the Mg/Si and Al/Si ratios, the barley grain dust can be discriminated from the corn

Element	ratio		
	Barley	Corn	Wheat
Mg/Si	4.0 ± 1.0	13.7 ± 5.0	22 ± 11
Al/Si	1.1 ± 0.3	9.4 ± 3.5	8 ± 4
Mg/Mn	4.6 ± 1.3	2.7 ± 1.1	1.3 ± 0.5
Na/Ca	0.76 ± 0.2	1.53 ± 0.2	0.3 ± 0.1
Al/Mn	1.3 ± 0.4	1.9 ± 0.9	0.45 ± 0.3
Si/Mn	1.2 ± 0.5	0.2 ± 0.07	0.06 ± 0.03
CN/C_2	2.9 ± 1.5	2.5 ± 1.3	3.0 ± 1.5
Mn/CN	0.14 ± 0.06	0.15 ± 0.07	0.35 ± 0.12
Al/CN	0.15 ± 0.02	0.23 ± 0.08	0.13 ± 0.07

TABLE 1 Line intensity ratios for the barley, corn, and wheat samples. The atomic lines and molecular bands selected are Mg I (285.17 nm), Si I (288.16 nm), Al I (396.15 nm), Mn I (403.31 nm), Ca I (422.67 nm), Na I (588.99 nm), CN (388.25 nm) and C_2 (516.41 nm)

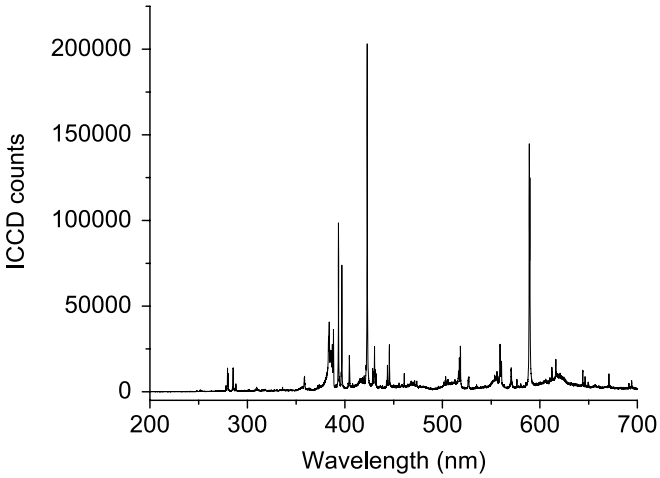

FIGURE 6 Time-resolved FIBS spectra obtained for barley grain dusts with the delay of $t = 60$ ns. Laser pulse energy is 95 mJ and the ICCD gate width is 2 μs

and wheat dusts, while from the Al/Mn and Si/Mn ratios, the wheat dust can easily be distinguished from the barley and corn dusts. In particular, the ratio of the most intense spectral lines, respectively Na (I) and Ca(I), are not the same for the samples and are quite easy to observe. Moreover, the error bars are small enough to distinguish them with only these two lines.

To show the feasibility of remote detection of biological samples, we also measured the fluorescence spectrum of barley by placing the sample in a corridor outside the laboratory at a distance of 50 m away from the laser and detection systems, as shown in Fig. 6. The time delay is $t = 60$ ns and the gate width is 2 μs. This experiment was performed with a laser energy of 95 mJ and a pulse duration of 10 ps. The diameter of the laser beam is 2.5 cm (FWHM). As can be seen in Fig. 6, the spectrum is very clean (no continuum), and all of the spectral lines shown in Fig. 2 can be clearly observable. Moreover, the line intensity ratios are in a good agreement (within the error bars) with the values obtained in the laboratory. This further demonstrates the feasibility of this technique for remote detection of biological samples.

4 Conclusions

In summary, the plasma emissions from barley, corn, and wheat grain dusts induced by filamentation in air

have been recorded in a Lidar configuration. The spectral analysis shows similar chemical compositions, but different element abundances of these three bioaerosols. The kinetic analysis of the CN and C_2 bands demonstrates that CN are due either to the production of native CN in the samples, or to the interaction of C_2 in the plasma with N_2 in the ambient air, while C_2 are derived directly from native C_2 production from the samples. The line intensity ratios have been used to distinguish these samples. Good reproducibility has also been obtained. This result, to our knowledge, shows for the first time that FIBS can be used to distinguish three examples of agricultural-activity related bioaerosols with so similar or almost identical composition. This opens important potential capabilities for military and civil applications to confirm with high probability the presence of biological threats using this technique. Clearly, FIBS has shown a good ability to remotely detect and distinguish three closely related types of bioaerosols. However, in view of the complex structures of biological agents, much effort is required to verify the capability of the technique to distinguish between numerous types of bioaerosols including simulants of biological agents.

ACKNOWLEDGEMENTS We would like to thank the technical support of M. Martin. This work was supported in part by the Natural Sciences and Engineering Research Council, Defence Research and Development Canada-Valcartier, Canada Foundation for Innovation, Femtotech, and Canada Research Chairs.

REFERENCES

1 L.G. Blevins, C.R. Shaddix, S.M. Sickafoose, P.M. Walsh, Appl. Opt. **42**, 6107 (2003)
2 A.K. Rai, F.Y. Yueh, J.P. Singh, Appl. Opt. **42**, 2078 (2003)
3 K.Y. Yamamoto, D.A. Cremers, M.J. Ferris, L.E. Foster, Appl. Spectrosc. **50**, 222 (1996)
4 M. Corsi, V. Palleschi, E. Tognoni (Eds.), Spectrochim. Acta B **56**, 565 (2001)
5 N. Omenetto, J.J. Lasema (Eds.), Spectrochim. Acta B **60**, 877 (2005)
6 R. Grönlund, M. Lundqvist, S. Svanberg, Opt. Lett. **30**, 2882 (2005)
7 A. Assion, M. Wollenhaupt, L. Hag, F. Mayorov, C. Sarpe-Tudoran, M. Winter, U. Kutschera, T. Baumert, Appl. Phys. B **77**, 391 (2003)
8 F. Courvoisier, V. Boutou, V. Wood, A. Bartelt, M. Roth, H. Rabitz, J.-P. Wolf, Appl. Phys. Lett. **87**, 063 901 (2005)
9 P. Rohwetter, J. Yu, G. Méjean, K. Stelmaszczyk, E. Salmon, J. Kasparian, J.-P. Wolf, L. Wöste, J. Anal. Atom. Spectrom. **19**, 437 (2004)
10 S.L. Chin, *From Multiphoton to Tunnel Ionization*, in: Advances in Multiphoton Processes and Spectroscopy, ed. by S.H. Lin, A.A. Villaeys, Y. Fujimura (World Scientific, Singapore, 2004), vol. 16, pp. 249–272
11 M. Baudelet, L. Guyon, J. Yu, J.-P. Wolf, T. Amodeo, E. Frejafon, P. Laloi, J. Appl. Phys. **99**, 084 701 (2006)
12 K. Stelmaszczyk, P. Rohwetter, G. Méjean, J. Yu, E. Salmon, J. Kasparian, R. Ackermann, J.-P. Wolf, L. Wöste, Appl. Phys. Lett. **85**, 3977 (2004)
13 S.L. Chin, S.A. Hosseini, W. Liu, Q. Luo, F. Théberge, N. Aközbek, A. Becker, V.P. Kandidov, O.G. Kosareva, H. Schroeder, Can. J. Phys. **83**, 863 (2005) and references therein
14 M. Rodriguez, R. Bourayou, G. Méjean, J. Kasparian, J. Yu, E. Salmon, A. Scholz, B. Stecklum, J. Eislöffel, U. Laux, P. Hatzes, R. Sauerbrey, L. Wöste, J.-P. Wolf, Phys. Rev. E **69**, 036 607 (2004)
15 K. Stelmaszczyk, P. Rohwetter, G. Méjean, J. Yu, E. Salmon, J. Kasparian, R. Ackermann, J.-P. Wolf, L. Wöste, Appl. Phys. Lett. **85**, 3977 (2004)
16 H.L. Xu, W. Liu, S.L. Chin, Opt. Lett. **31**, 1540 (2006)
17 S. Morel, N. Leone, P. Adam, J. Amouroux, Appl. Opt. **42**, 6184 (2003)
18 C.A. Munson, F.C. De Lucia Jr., T. Piehler, K.L. McNesby, A.W. Miziolek, Spectrochim. Acta B **60**, 1217 (2005)
19 M. Baudelet, L. Guyon, J. Yu, J.-P. Wolf, T. Amodeo, E. Frejafon, P. Laloi, Appl. Phys. Lett. **88**, 063 901 (2006)
20 S.L. Chin, A. Brodeur, S. Petit, O.G. Kosareva, V.P. Kandidov, J. Nonlinear Opt. Phys. Mater. **8**, 121 (1999)
21 V.P. Kandidov, O.G. Kosareva, I.S. Golubtsov, W. Liu, A. Becker, N. Aközbek, C.M. Bowden, S.L. Chin, Appl. Phys. B **77**, 149 (2003)
22 N. Aközbek, A. Iwasaki, A. Becker, M. Scalora, S.L. Chin, C.M. Bowden, Phys. Rev. Lett. **89**, 143 901 (2002)
23 NIST Database; see http://physics.nist.gov/cgi-bin/AtData/lines_form
24 R.W.B. Pearse, A.G. Gaydon, *The Identification of Molecular Spectra* (Chapman and Hall, New York, 1976)
25 H.L. Xu, J.F. Daigle, Q. Luo, S.L. Chin, Appl. Phys. B **82**, 655 (2006)
26 C. Aragón, J.A. Aguilera, F. Peñalba, Appl. Spectrosc. **53**, 1259 (1999)